ARMY RESEARCH LABORATORY

Topics in Computational Modeling of Shock and Wave Propagation

by George A. Gazonas

ARL-SR-145 **September 2006**

NOTICES

Disclaimers

The findings in this report are not to be construed as an official Department of the Army position unless so designated by other authorized documents.

Citation of manufacturer's or trade names does not constitute an official endorsement or approval of the use thereof.

Destroy this report when it is no longer needed. Do not return it to the originator.

Army Research Laboratory
Aberdeen Proving Ground, MD 21005-5069

ARL-SR-145 **September 2006**

Topics in Computational Modeling of Shock and Wave Propagation

George A. Gazonas
Weapons and Materials Research Directorate, ARL

REPORT DOCUMENTATION PAGE

Form Approved
OMB No. 0704-0188

1. REPORT DATE *(DD-MM-YYYY)*	2. REPORT TYPE	3. DATES COVERED (From - To)
September 2006	Final	July 2004–July 2005

4. TITLE AND SUBTITLE
Topics in Computational Modeling of Shock and Wave Propagation

5a. CONTRACT NUMBER

5b. GRANT NUMBER

5c. PROGRAM ELEMENT NUMBER

6. AUTHOR(S)
George A. Gazonas

5d. PROJECT NUMBER
62105AH84

5e. TASK NUMBER

5f. WORK UNIT NUMBER

7. PERFORMING ORGANIZATION NAME(S) AND ADDRESS(ES)
U.S. Army Research Laboratory
ATTN: AMSRD-ARL-WM-MD
Aberdeen Proving Ground, MD 21005-5069

8. PERFORMING ORGANIZATION REPORT NUMBER
ARL-SR-145

9. SPONSORING/MONITORING AGENCY NAME(S) AND ADDRESS(ES)

10. SPONSOR/MONITOR'S ACRONYM(S)

11. SPONSOR/MONITOR'S REPORT NUMBER(S)

12. DISTRIBUTION/AVAILABILITY STATEMENT
Approved for public release; distribution is unlimited.

13. SUPPLEMENTARY NOTES

14. ABSTRACT
This report addresses several practical problems related to computational modeling of shock and wave propagation in cellular, viscoelastic, microcracked, and fragmented media. “Impulsive Loading of Cellular Media in Sandwich Construction” derives an analytical model for a cellular medium subjected to blast and examines the influence of the relative distribution of mass among the cellular core and the front and back faces of the sandwich structure. “Transient Stress Optimization of Elastic and Viscoelastic Composite Strips” examines wave propagation in elastic and viscoelastic layered media, with the goal of minimizing stress amplitude in the layers. Solutions to initial boundary value problems are obtained via Laplace transform methods using a modified Dubner-Abate-Crump algorithm. “Numerical Modeling of Wave Propagation in Anisotropically Microcracked Media” utilizes a generalized self-consistent method to evaluate the effective moduli in microcracked media. Slowness diagrams illustrate key features of the anisotropic nature of the quasi-longitudinal and shear wave speeds in microcracked media subjected to either a far-field compressive or tensile load. Finally, “Numerical Convergence of the Cohesive Element Approach in Dynamic Fragmentation Simulations” solves a long-standing problem related to energy convergence in numerical simulations of fragmentation in brittle materials. It is shown that a random finite-element mesh spacing leads to much faster and smoother convergence of the dissipated cohesive energy than uniform meshes.

15. SUBJECT TERMS
blast loading, cellular media, viscoelastic composites, effective moduli, microcrack damage, fragmentation, cohesive element

16. SECURITY CLASSIFICATION OF:			17. LIMITATION OF ABSTRACT	18. NUMBER OF PAGES	19a. NAME OF RESPONSIBLE PERSON
a. REPORT	b. ABSTRACT	c. THIS PAGE			George A. Gazonas
UNCLASSIFIED	UNCLASSIFIED	UNCLASSIFIED	UL	30	19b. TELEPHONE NUMBER (*Include area code*) 410-306-0863

Preface

This report contains reprints of four papers* that focus on various aspects of shock and wave propagation in cellular, viscoelastic, microcracked, and fragmented media that appear in the *Proceedings of the Conference of the American Physical Society Topical Group on Shock Compression of Condensed Matter*, Baltimore, MD, 31 July–5 August 2005.

*Main, J. A.; Gazonas, G. A. Impulsive Loading of Cellular Media in Sandwich Construction. CP845, *Shock Compression of Condensed Matter – 2005*; Furnish, M. D., Elert, M., Russell, T. P., White, C. T., Eds.; American Institute of Physics, pp 1539–1542, 2006.

*Laverty, R.; Gazonas, G. A. Transient Stress Optimization of Elastic and Viscoelastic Composite Strips. CP845, *Shock Compression of Condensed Matter – 2005*; Furnish, M. D., Elert, M., Russell, T. P., White, C. T., Eds.; American Institute of Physics, pp 1535–1538, 2006.

*Su, D.; Santare, M. J.; Gazonas, G. A. Numerical Modeling of Wave Propagation in Anisotropically Microcracked Media. CP845, *Shock Compression of Condensed Matter – 2005*; Furnish, M. D., Elert, M., Russell, T. P., White, C. T., Eds.; American Institute of Physics, pp 359–362, 2006.

*Raghupathy, R.; Gazonas, G. A.; Molinari, J. F.; Zhou, F. Numerical Convergence of the Cohesive Element Approach in Dynamic Fragmentation Simulations. CP845, *Shock Compression of Condensed Matter – 2005*; Furnish, M. D., Elert, M., Russell, T. P., White, C. T., Eds.; American Institute of Physics, pp 654–657, 2006.

INTENTIONALLY LEFT BLANK.

CP845, *Shock Compression of Condensed Matter - 2005,*
edited by M. D. Furnish, M. Elert, T. P. Russell, and C. T. White
2006 American Institute of Physics 0-7354-0341-4/06/$23.00

IMPULSIVE LOADING OF CELLULAR MEDIA IN SANDWICH CONSTRUCTION

Joseph A. Main[1] **and George A. Gazonas**[2]

[1]*Building and Fire Research Laboratory, National Institute of Standards and Technology*
100 Bureau Drive, Mail Stop 8611, Gaithersburg, MD 20899-8611
[2]*Weapons and Materials Research Directorate, U.S. Army Research Laboratory*
ATTN: AMSRD-ARL-WM-MD, Aberdeen Proving Ground, MD 21005-5069

Abstract. Motivated by recent efforts to mitigate blast loading using energy-absorbing materials, this paper investigates the uniaxial crushing of cellular media in sandwich construction under impulsive pressure loading. The cellular core is modeled using a rigid, perfectly-plastic, locking idealization, as in previous studies, and the front and back faces are modeled as rigid, with pressure loading applied to the front face and the back face unrestrained. Predictions of this analytical model show excellent agreement with explicit finite element computations, and the model is used to investigate the influence of the mass distribution between the core and the faces. Increasing the mass fraction in the front face is found to increase the impulse required for complete crushing of the cellular core but also to produce undesirable increases in back-face accelerations. Optimal mass distributions are investigated by maximizing the impulse capacity while limiting the back-face accelerations to a specified level.

Keywords: Blast mitigation, aluminum foam, shock wave, finite element analysis.
PACS: 46.40.Cd, 62.50.+p, 83.60.Uv.

BACKGROUND

Cellular materials such as metal foams and honeycombs are being considered in a wide variety of structural applications because of their capacity to absorb impact energy. Surprisingly, however, their use under blast loading has often led to enhancement, rather than mitigation, of blast effects. Experiments by Hanssen et al. [1] showed that increased upswing results from the addition of an aluminum foam layer to the face of a massive "pendulum" subjected to blast loading. Nesterenko [2] noted that in these experiments, the blast impulse is imparted primarily to a lightweight plate covering the foam layer, leading to significantly higher kinetic energy than if the same impulse were imparted directly to the more massive pendulum. Xue and Hutchinson [3] noted a similar effect in a computational study of blast loading on sandwich plates, in which the kinetic energy imparted to a sandwich plate was observed to be greater than for a solid plate of the same mass. In spite of this, it was found that deflections of sandwich plates could be significantly less than for the corresponding solid plate. Xue and Hutchinson considered front and back face sheets with equal mass but suggested that further reductions in deflections might be achieved by increasing the mass fraction in the face sheet near the blast.

ANALYTICAL MODEL

Motivated by these observations, an analytical model is developed in this paper to investigate the influence of mass distribution on the uniaxial crushing of cellular material sandwiched between

rigid layers. The cellular core material is represented by the simplified stress-strain relationship shown in Fig. 1(b), originally proposed by Reid and Peng [4] for modeling crushing of wood and subsequently applied to cellular metals in a number of studies (e.g., [1,5]). Arbitrary masses of the front and back faces are permitted, and a pressure pulse $p(t)$ is applied to the front face with the back face unrestrained. This sandwich model is a generalization of that in [1], which considered a fixed back face, and of that in [5], which considered front and back faces of equal mass with blast loading represented by an initial velocity imparted to the front face.

A strip of sandwich panel with unit cross-sectional area is considered, with total mass given by $m = m_1 + \rho_0 \ell_0 + m_2$, where ρ_0 and ℓ_0 are the uncompressed density and thickness of the cellular core, and m_1 and m_2 are the areal densities of the front and back faces. The acceleration of the center of mass, denoted $\ddot{u}_G$, follows directly from application of Newton's second law to the strip:

$$p(t) = m\ddot{u}_G \tag{1}$$

Provided the applied pressure is sufficiently high, densification of the cellular core commences at the front face, and a densification front propagates through the core. By conservation of mass, the density of the compressed core material is $\rho_0/(1-\varepsilon_0)$. According to the simplified model of Fig. 1(b), the compressed core material moves as a rigid body with the same velocity as the front face, denoted $\dot{u}_1$, while the uncompressed core material moves as a rigid body with the velocity of the back face, $\dot{u}_2$. The stress just ahead of the densification front is σ_0, and application of Newton's second law to the material ahead of the densification front then yields the following equation:

$$\sigma_0 = (\rho_0 x + m_2)\ddot{u}_2 \tag{2}$$

where x denotes the thickness of the uncompressed core material, and the thickness of the densification front itself is assumed to be negligible. By forming and differentiating an expression for x_G, the distance of the center of mass from the back face, it follows that

$$\ddot{x}_G = (\varepsilon_0 / m)\left\{\left[m_1 + \rho_0(\ell_0 - x)\right]\ddot{x} - \rho_0 \dot{x}^2\right\} \tag{3}$$

Eqs. (1) - (3) can then be combined through the relation $\ddot{u}_2 = \ddot{u}_G + \ddot{x}_G$ to yield the following nonlinear ordinary differential equation for x:

$$\begin{aligned} -\varepsilon_0\left[m_1 + \rho_0(\ell_0 - x)\right]\ddot{x} + \varepsilon_0\rho_0\dot{x}^2 \\ = p(t) - \sigma_0\, m/(\rho_0 x + m_2) \end{aligned} \tag{4}$$

Eq. (4) can be integrated numerically with initial conditions $x(0) = \ell_0$ and $\dot{x}(0) = 0$. A triangular pressure pulse is considered, as shown in Fig. 1(c), with total impulse denoted i_∞. The following symbols are introduced to denote the nondimensional peak pressure and total impulse:

$$P_0 = \frac{p_0}{\sigma_0};\ I_\infty = \frac{i_\infty}{m}\sqrt{\frac{\rho_0}{\sigma_0 \varepsilon_0}} \tag{5}$$

The following symbols denote the mass fractions in the core and in the front and back faces:

$$\eta_0 = \rho_0 \ell_0 / m;\ \eta_1 = m_1 / m;\ \eta_2 = m_2 / m \tag{6}$$

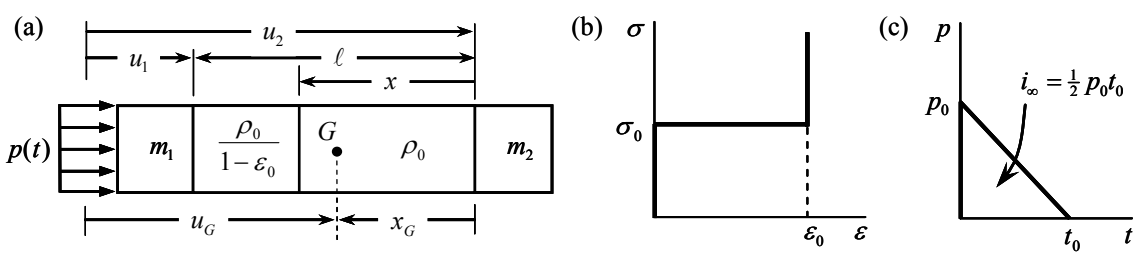

Figure 1. Analytical model definition: (a) Strip of sandwich panel with partially compacted core; (b) Stress vs. volumetric strain relationship for core material; (c) Triangular pressure pulse applied to front face.

Table 1. Parameters of computational simulations.

Case	η_1	η_0	η_2	P_0	I_∞
pendulum	0.0125	0.0125	0.975	10	0.015
sandwich	0.25	0.5	0.25	10	1

COMPARISON WITH COMPUTATIONS

The predictions of the analytical model are compared with explicit finite element computations using LS-DYNA. In the computations, the cellular core was represented by a single row of solid elements with total thickness ℓ_0 = 5 cm, using material model 26 (*MAT_HONEYCOMB) with ρ_0 = 250 kg/m^3, σ_0 = 1 MPa, and ε_0 = 0.7. A large elastic modulus of E = 700 GPa was used to represent the "rigid" portions of the idealized stress-strain relationship in Fig. 1(b), and Poisson's ratio was set to zero. The material viscosity coefficient μ was set to 0.001, and 150 elements were found to be sufficient for convergence.

The front and back faces were represented in the computations by added nodal masses, and two different mass distributions were considered, as indicated in Table 1. The "pendulum" case corresponds to the blast pendulum experiments of [1], with the large back-face mass representing the pendulum. The "sandwich" case corresponds to the sandwich plates of [3] and [5], with equal front-face and back-face masses.

In Figs. 2 and 3, computational results are compared with predictions of the analytical model, and good agreement is observed. Results are plotted against nondimensional time, $\tau = (\sigma_0 / i_\infty)t$. The nondimensional velocities in Figs. 2 and 3 are defined as $\bar{v}_1 = \dot{u}_1 / v_\infty$ and $\bar{v}_2 = \dot{u}_2 / v_\infty$, where $v_\infty = i_\infty / m$ is the final velocity of the center of mass. Due to the small mass of the front face, much larger nondimensional front-face velocities are observed in the "pendulum" case, despite the much smaller nondimensional impulse I_∞ in this case, as shown in Table 1.

INFLUENCE OF MASS DISTRIBUTION

Fig. 3(a) shows contours of the critical nondimensional impulse I_∞ for which complete densification of the core is first achieved. These contours correspond to the limiting case of a Dirac delta impulse ($P_0 \to \infty$) and were obtained by numerical solution of Eq. (4). Fig. 3(a) shows that increasing the mass fraction in the core and in the front face increases the impulse capacity of the sandwich system. However, Fig. 3(b) shows that increasing the mass fraction in the core and in the front face also leads to increased back-face accelerations, thus sacrificing a protective function of the cellular core. The nondimensional back-face accelerations presented in Fig. 3(b) are defined as $\bar{a}_2 = (m/\sigma_0)\ddot{u}_2$. It follows from Eq. (2) that the peak back-face accelerations occur at the instant of complete compaction (x = 0), for which $\ddot{u}_2 = \sigma_0 / m_2$ or $\bar{a}_2 = 1/\eta_2$. A design optimization problem can be posed by seeking to maximize the impulse I_∞ that can be sustained while limiting the back-face accelerations to a specified level. Fig. 4 shows a contour plot of the maximum impulse I_∞ that can be sustained with accelerations limited to $\bar{a}_2 = 5$. The grey curve in Fig. 4 corresponds to $1/\eta_2 = 5$. Below this curve, the values of

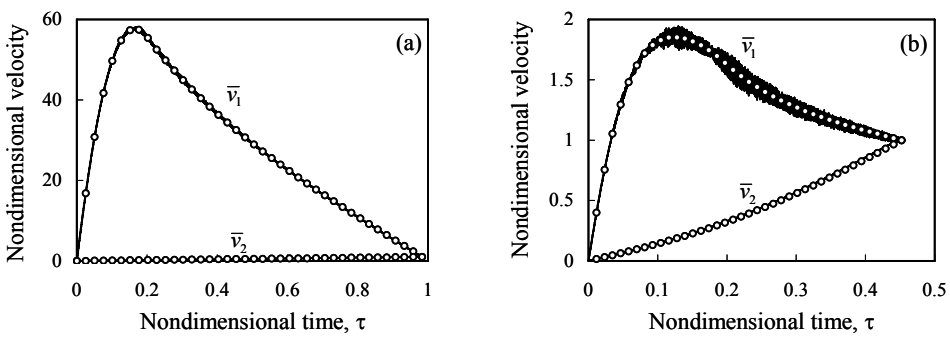

Figure 2. Comparison of LS-DYNA computations (—) with predictions of analytical model (○): Nondimensional front-face and back-face velocities for (a) "pendulum" case; (b) "sandwich" case.

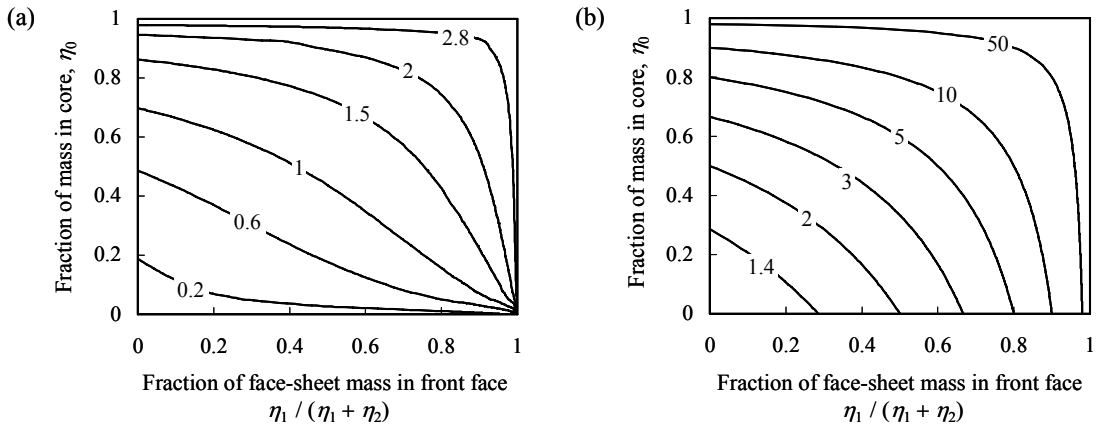

Figure 3. Contours with varying mass distribution: (a) Critical nondimensional impulse I_∞ required for complete compaction of core ($P_0 \to \infty$); (b) Peak nondimensional back-face acceleration $\bar{a}_2$ at complete compaction of core.

maximum impulse correspond to complete compaction of the core and are the same as in Fig. 3(a). Above this curve, $\bar{a}_2 > 5$ at complete compaction, so only partial compaction is permitted and the values of maximum impulse are less than in Fig. 3(a). In the shaded region of Fig. 4, defined by $(\eta_0 + \eta_2)^{-1} > 5$, $\bar{a}_2 > 5$ at initiation of compaction, so the maximum allowable impulse is zero. It is evident in Fig. 4 that for a given mass fraction in the core η_0, the allowable impulse is maximized along the grey curve, i.e., by adjusting the mass distribution so that the acceleration at complete compaction equals the allowable value.

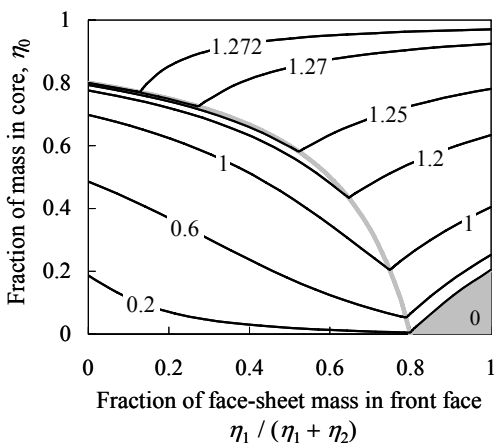

Figure 4. Contours of maximum nondimensional impulse I_∞ with nondimensional back-face accelerations limited to $\bar{a}_2 = 5$.

ACKNOWLEDGEMENTS

This work was supported in part by an appointment of the first author to the Postgraduate Research Participation Program at the U.S. Army Research Laboratory (ARL) administered by the Oak Ridge Institute for Science and Education through an interagency agreement between the Department of Energy and ARL.

REFERENCES

1. Hanssen, A. G., Enstock, L., and Langseth, M. "Close-range blast loading of aluminum foam panels." *Int. J. Impact Eng.* **27**, 593-618 (2002).
2. Nesterenko, V. F. "Shock (blast) mitigation by 'soft' condensed matter." *MRS Proceedings*, Vol. 759 (2002).
3. Xue, Z. and Hutchinson, J. W. "Preliminary assessment of sandwich plates subject to blast loads." *Int. J. Mech. Sci.* **45**, 687-705 (2003).
4. Reid, S. R. and Peng, C. "Dynamic uniaxial crushing of wood." *Int. J. Impact Eng.* **19**, 531-570 (1997).
5. Fleck, N. A. and Deshpande, V. S. "The resistance of clamped sandwich beams to shock loading." *J. Appl. Mech.* **71**, 386-401 (2004).

Certain trade names or company products are mentioned in the text to specify adequately the procedure used. Such identification does not imply recommendation or endorsement by NIST or ARL, nor does it imply that the product is the best available for the purpose.

CP845, *Shock Compression of Condensed Matter - 2005,*
edited by M. D. Furnish, M. Elert, T. P. Russell, and C. T. White
2006 American Institute of Physics 0-7354-0341-4/06/$23.00

TRANSIENT STRESS OPTIMZATION OF ELASTIC AND VISCOELASTIC COMPOSITE STRIPS

Rich Laverty[1], and George Gazonas[2]

[1] Department of Mathematics, Juniata College, Juniata, PA 16652
[2]WMRD, US Army Research Laboratory, Aberdeen Proving Ground, MD 21005-5069

Abstract. In this study we examine transient stresses in elastic and viscoelastic composite strips. When the stress is the result of a stress step we seek combinations of material parameters that lead to a minimum peak stress in the layer most distant from the applied stress. In the case of impact by a rigid body we define an optimal design as one in which the maximum stress is achieved in the layer subject to the impact. The primary purpose of these results is benchmarking larger numerical studies coupling a finite element code (DYNA3D) with several optimization routines.

Keywords: Elastic Waves, Viscoelastic Waves, Optimization, Inverse Laplace Transform.
PACS: 62.30.+d, 43.20.Gp, 83.60.Bc

INTRO

Design of stress wave attenuators is a computationally expensive task with few analytic solutions. Therefore, there are almost no benchmarks for the larger, more complex computations. The purpose of this study is to find reliable solutions to transient wave propagation in one-dimensional composite strips. These solutions are examined for possible optimal designs.

First, we introduce the idea of an optimal design by considering elastic strips. The following sections consider viscoelastic strips, and altering the applied stress to low-velocity impact.

ELASTIC STRIPS

For comparison, we report the relevant result from a homogenous strip of an elastic material. This will be used to benchmark the performance of composites.

Homogeneous Elastic Strip

Consider an elastic material occupying $0 < x < L$, initially at rest, and fixed on the right ($x = L$). Upon application of a stress step on the left, stress propagates through material; hereafter, referred to as a strip. The mathematical model of this is the Initial Boundary Value Problem (IBVP):

$$\begin{aligned} &\partial_{tt}u = c^2\partial_{xx}u \\ &0 = u(x,0), \quad 0 = \partial_t u(x,0) \\ &\sigma_0 H(t) = E\partial_x u(0,t) \\ &0 = u(L,t) \end{aligned}, \qquad (1)$$

where u is the displacement, σ_0 the magnitude of the applied stress, $H(t)$ the Heaviside step function, E the elastic modulus, and ρ the density of the strip. The speed of stress waves is $c = \sqrt{E/\rho}$.

Fig. 1 is a stress history at two points along the strip, $x = L/4$ and $3L/4$. These points were chosen because they will be the midpoints of the layers of the composite.

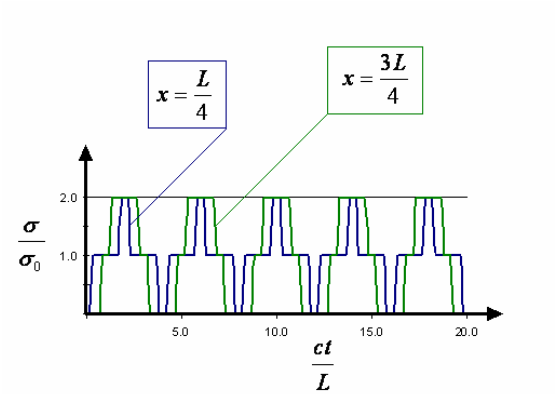

Figure 1. The stress history measured at two points of the homogeneous elastic strip.

The relevant feature of Fig. 1 is the peak stress. At each point of measurement the maximum stress is $2\sigma_0$.

Two Layered Elastic Strip

Now consider a strip composed of two layers. Layer 1 occupies $0 < x < L/2$ and layer 2, $L/2 < x < L$. All quantities, displacement, stress, density and elastic modulus, will have their corresponding layer indicated by a subscript. The displacements in each layer, u_i, obeys the partial differential equation and initial conditions in (1). The boundary conditions of (1) are replaced by

$$\begin{aligned} \sigma_0 H(t) &= E\partial_x u_1(x,0) \\ 0 &= u_2(L,t) \end{aligned} \quad . \qquad (2)$$

To complete the model we need interface conditions. We assume that the displacement and stress are continuous at the layer interface,

$$\begin{aligned} u_1(L/2-,t) &= u_2(L/2+,t) \\ E_1\partial_x u_1(L/2-,t) &= E_2\partial_x u_2(L/2+,t) \end{aligned} \quad . \qquad (3)$$

We restrict our attention to materials where the elastic modulus and density in layer 2 are scaled from their values in layer 1 by the same factor, α.

$$E_2 = E_1/\alpha, \quad \rho_2 = \rho_1/\alpha \, . \qquad (4)$$

This implies $c_1 = c_2$, so we drop the subscript.

Fig. 2 is a comparison of stress histories at $x = 3L/4$ for the homogeneous strip and a composite with $\alpha = 1.1$. In contrast with Fig. 1, the stress in the composite exceeds $2\sigma_0$.

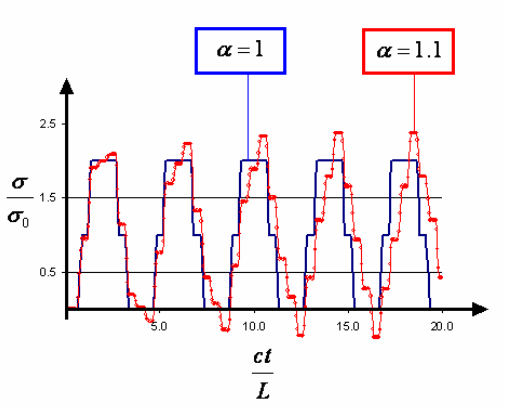

Figure 2. Stress measured at $x = 3L/4$ for $\alpha = 1$ (homogeneous strip), and $\alpha = 1.1$.

This phenomenon is common for almost all composite strips. In [1] an analytic solution is constructed for the IBVP of the composite. It was shown that the stress amplitude in layer 2 will exceed $2\sigma_0$ in all but a discrete set of designs. These 'optimal' designs occur when

$$\alpha = \frac{1+\cos(\pi/k)}{1-\cos(\pi/k)}, \quad k = 2,3,\ldots \qquad (5)$$

For optimal designs the peak stress in layer 2 will be $2\sigma_0$. Fig. 3 shows the peak stress, in layers 1 and 2, as α varies. Optimal designs are visible.

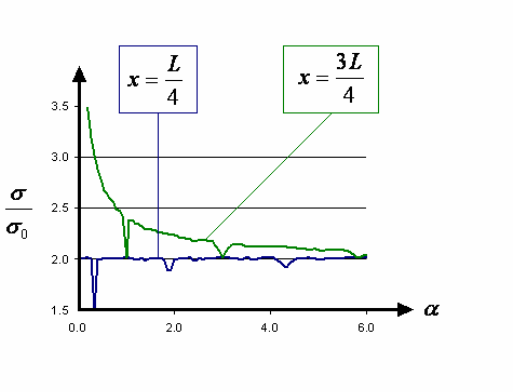

Figure 3. Peak stress measured at two points of the composite strip as α is varied.

In the following, we seek results similar to Fig. 3. We will consider viscoelastic strips and elastic strips subject to low-velocity impacts.

VISCOELASTIC STRIPS

For a strip composed of viscoelastic layers the IBVP (1) must be adjusted. We keep the notation of denoting quantities in each layer with subscripts. The equation of motion and initial conditions are

$$\begin{aligned} &\rho_i \partial_{tt} u_i = \partial_x \sigma_i \\ &0 = u_i(x,0), \quad 0 = \partial_t u_i(x,0) \end{aligned} . \tag{6}$$

The boundary and interface conditions are

$$\begin{aligned} &\sigma_0 H(t) = \sigma_1(0,t) \\ &0 = u_2(L,t) \\ &u_1(L/2-,t) = u_2(L/2+,t) \\ &\sigma_1(L/2-,t) = \sigma_2(L/2+,t) \end{aligned} . \tag{7}$$

The complete problem statement includes the constitutive relationship

$$\sigma_i(x,t) = \int_0^t G_i(t-\tau)\partial_{x\tau} u_i(x,\tau)\,d\tau , \tag{8}$$

where $G_i(t)$ is the relaxation modulus of layer i. We restrict our attention to standard linear solids

$$G_i(t) = G_{i,\infty} + (G_{i,0} - G_{i,\infty})e^{-\beta_i t} . \tag{9}$$

$G_{i,0}$ is the initial elastic response of the material, $G_{i,\infty}$ the long term stress response, and β_i the decay parameter.

We make the following parameter choices.

$$\begin{aligned} &G_{1,0} = E, \quad G_{2,0} = E/\alpha \\ &G_{i,\infty} = G_{i,0}/2, \quad \rho_2 = \rho_1/\alpha \end{aligned} \tag{10}$$

The speed of propagation in each layer, $c_i = \sqrt{G_{i,0}/\rho_i}$, is the same and will be denoted by c.

The decay parameter is a viscosity measure. Materials with small β will behave similarly to elastic materials when considering transient stresses. We have chosen β_i the same in each layer, so its subscript has been dropped.

Equations (6) through (9) comprise an integro-differential equation for the propagation of stress waves in the strip. Due to its complicated nature, this IBVP is solved numerically using the Laplace transform with a modified DAC algorithm for inversion, [2,3,4]. The results for different values of α and three values β are displayed in Fig. 4.

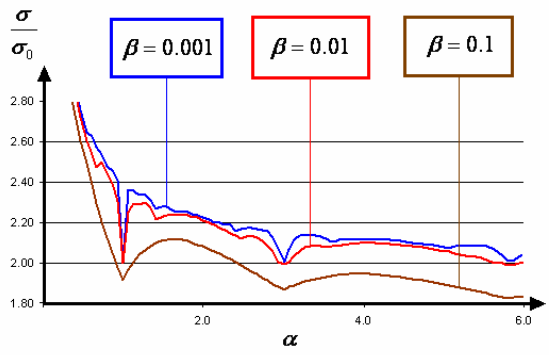

Figure 4. Peak stress at $x = 3L/4$ as α varies.

In Fig. 4 we see that as α varies the peak stress in layer 2 behaves similar to the elastic composite. In fact, when β is small the results are almost indistinguishable from the elastic case. As β increases the viscous nature of the solid becomes more pronounced and the difference between optimal and nearby designs becomes less dramatic.

LOW VELOCITY IMPACT

Now reconsider the two layered elastic strip in (1) through (4), but replace the stress step with the impact of another solid.

Consider a rigid body of mass m moving to the right with a velocity $v_0 < c$. The impact is modeled by coupling the position of the right of the rigid body, $u_0(t)$, with the stress in the strip through the condition

$$m\partial_{tt}u_0(t) = E_1\partial_x u_1(0,t). \qquad (11)$$

Fig. 5 contains the results from this IBVP using the characteristic stress

$$\sigma_0 = v_0\sqrt{E_1\rho_1}\,. \qquad (12)$$

Optimal designs similar to those in Fig. 3 don't exist. However, we do see that the stress in layer 2 is the lowest stress when α is greater than 1. This corresponds to a composite with a stiffer layer 1.

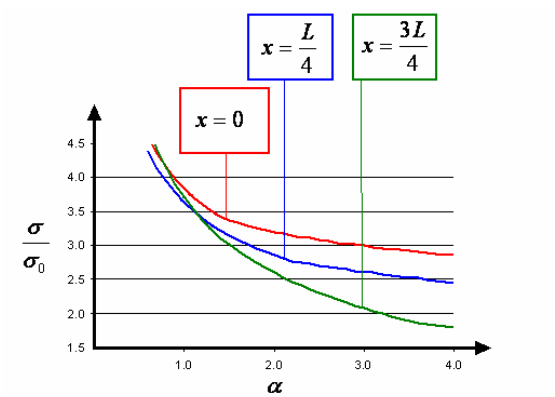

Figure 5. Peak stress at the point of contact and the midpoint of each layer.

CONCLUSIONS

The optimal designs of composite elastic strips can be extended to strips composed of viscoelastic materials, with similar results. When low velocity impacts replace stress steps the optimizability is lost. However, a lower peak stress is recorded in the layer 2 when the front layer is the stiffer of the two. Though not optimal, this is still a desirable property for a stress wave attenuator.

ACKNOWLEDGEMENTS

This work was performed while Rich Laverty held a National Research Council Research Associateship Award at the Army Research Lab and the United States Military Academy.

REFERENCES

1. Velo, A. and Gazonas, G., "Optimal design of a two-layered elastic strip subject to transient loading," IJSS, Vol. 56, no. 7, pp. 1-10, 2003.
2. Laverty, R. and Gazonas, G., "Laplace Transform Inversion and Viscoelastic Wave Propagation", in Proceedings of the 11th Annual ARL/USMA Technical Symposium, pp. 1-24, 2003.
3. Laverty, R. and Gazonas, G., "Transient Stress Analysis of Elastic-Viscoelastic Strips Subject to Impact Loads", in Proceedings of the 12th Annual ARL/USMA Technical Symposium, pp. 1-16, 2004.
4. Laverty, R. and Gazonas, R., "An Improvement to the Fourier Series Method for the Inversion of Laplace Transforms Applied to Elastic and Viscoelastic Waves", to appear in IJCM.

CP845, *Shock Compression of Condensed Matter - 2005,*
edited by M. D. Furnish, M. Elert, T. P. Russell, and C. T. White
2006 American Institute of Physics 0-7354-0341-4/06/$23.00

NUMERICAL MODELING OF WAVE PROPAGATION IN ANISOTROPICALLY MICROCRACKED MEDIA

Dan Su[1], Michael H. Santare[1], George A. Gazonas[2]

[1]*Center for Composite Materials and Department of Mechanical Engineering, University of Delaware, Newark, DE, 19716*
[2] *U.S. Army Research Laboratory, Aberdeen Proving Ground, MD, 21005*

Abstract. A generalized self-consistent method (GSCM) is used to evaluate the effective moduli of a cracked medium and the wave propagation speed within this medium. Since the microcrack damage will in general have an angular distribution, the wave speed will be anisotropic. Furthermore, since cracks respond differently under tensile and compressive loads, waves propagating through the medium under different loading conditions will experience different wave speeds.

Keywords: Microcrack, Anisotropic, Wave, Effective moduli
PACS: 46.50.+a, 46.40.Cd, 83.60.Uv

INTRODUCTION

A number of problems of physical significance involve waves propagating through cracked media. Examples include seismic waves traveling through the earth's crust, the impact response of protective armor, and ultrasonic damage detection. The microcracks affect both the static properties of the medium and the way in which stress waves propagate.

When the wavelength is the same order of magnitude as the crack length, the waves will interact with individual cracks. There are many papers in the literature discussing this topic. In this study, we are interested in the problem when the wavelength is much larger than the crack length, allowing us to focus on how the damage affects the wave speed in the material.

In order to calculate the elastic wave propagation speed, we need to know the effective moduli of the cracked media. Many researchers have proposed different methods to evaluate the effective moduli of the cracked media, including the Self Consistent Method (Budiansky and O'Connell [1], Horii and Nemat-Nasser [2]), Mori-Tanaka [3] method (Benveniste [4]), Differential Scheme Method (Hashin [5]), generalized self-consistent method (Aboudi et al. [6], Huang et al. [7], Santare et al. [8]) and the effective self-consistent method (Zheng et al.[9]). We will use the anisotropic GSCM discussed in Santare et al. [8]

Sayers and Kachanov [10,11] studied microcrack induced elastic wave anisotropy. These papers connect the effective moduli of a cracked medium to the elastic wave speed. The authors use second-rank and fourth-rank crack density tensors to evaluate the effective elastic moduli. Using these, they calculate the effective moduli for perfectly aligned and randomly oriented crack distributions. Following these results, Schubnel and Gueguen [12,13] used micromechanical and statistical physics to evaluate the elastic wave velocities and permeability of cracked rocks.

Most of the above results are only applied to randomly oriented or perfectly aligned cracks. And only one of them (Horii and Nemat-Nasser [2])

considers the difference between tension and compression. This paper will investigate the difference between elastic wave propagation under tension and compression loads within a microcrack-damaged medium.

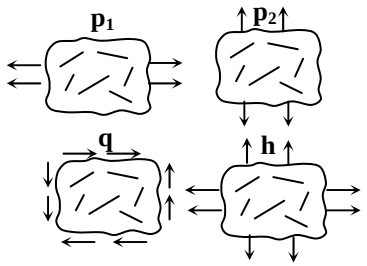

Figure 1. Four load cases

ANISOTROPIC EFFECTIVE MODULI OF MICROCRACKED MEDIA

Following Santare et al., [8] we use an anisotropic Generalized Self-Consistent Method GSCM to evaluate the effective moduli of the cracked medium. The GSCM equates the strain energy in a damaged region to the sum of the strain energy in the region if there were no damage plus the energy associated with the opening of the microcracks.

In a general, linear 2D orthotropic problem, there are four independent material constants. In order to evaluate these constants, we apply four separate load cases to the damaged region as shown in Fig. 1. Applying the energy balance to each of these cases and ignoring the effects of friction, results in four coupled equations [8] for the corresponding effective moduli $\boldsymbol{E}_1^*$, $\boldsymbol{E}_2^*$, μ^* and $\boldsymbol{K}^*$.

$$\frac{1}{\boldsymbol{E}_1^*}\boldsymbol{p}_1^2\boldsymbol{A}=\frac{1}{\boldsymbol{E}}\boldsymbol{p}_1^2\boldsymbol{A}+\sum_{k=1}^{M}\int_{C_k}[\boldsymbol{u}_i]^{p_1}\boldsymbol{t}_i^{p_1}d\boldsymbol{C}_k \qquad (1)$$

$$\frac{1}{\boldsymbol{E}_2^*}\boldsymbol{p}_2^2\boldsymbol{A}=\frac{1}{\boldsymbol{E}}\boldsymbol{p}_2^2\boldsymbol{A}+\sum_{k=1}^{M}\int_{C_k}[\boldsymbol{u}_i]^{p_2}\boldsymbol{t}_i^{p_2}d\boldsymbol{C}_k \qquad (2)$$

$$\frac{1}{\mu^*}\boldsymbol{q}^2\boldsymbol{A}=\frac{1}{\mu}\boldsymbol{q}^2\boldsymbol{A}+\sum_{k=1}^{M}\int_{C_k}[\boldsymbol{u}_i]^{q}\boldsymbol{t}_i^{q}d\boldsymbol{C}_k \qquad (3)$$

$$\frac{1}{\boldsymbol{K}^*}\boldsymbol{h}^2\boldsymbol{A}=\frac{1}{\boldsymbol{K}}\boldsymbol{h}^2\boldsymbol{A}+\sum_{k=1}^{M}\int_{C_k}[\boldsymbol{u}_i]^{h}\boldsymbol{t}_i^{h}d\boldsymbol{C}_k \qquad (4)$$

Here $\boldsymbol{E}$, μ, $\boldsymbol{K}$ and are the undamaged moduli. $[\boldsymbol{u}_i]$ and t_i are the load-specific displacement jump and traction along each of the M cracks in the region of area A. The external loads p_1, p_2, h and q are defined in Fig 1.

Notice that if the loads in Fig. 1 are made compressive, most cracks will not open in Mode I, thus changing the energy terms in Eqs. (1)-(4). A linear solution will not pick up the physical difference between cracks opening in tension and closing in compression. Consequently, a linear model will predict the same moduli in tension and compression. To account for crack face contact, a finite element model, with nonlinear contact elements is used. This, in turn, will result in very different effective moduli for the medium when it is loaded in compression than when in tension. For this initial study, the friction associated with the contact is assumed zero.

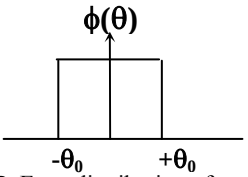

Figure 2. Even distribution of cracks

In both tension and compression, the resulting effective moduli will be affected by two properties of the microcrack array, its crack density and its orientation. The crack density is characterized by $\eta=\boldsymbol{M}\boldsymbol{c}^2/\boldsymbol{A}$ where c is the average half crack length. The orientation is characterized by a probability distribution around a mean orientation. Here, the average orientation is taken to be parallel to the x-axis and the individual crack angle is θ. The distribution is then taken to be constant from $-\theta_0$ to θ_0 as shown in Fig. 2. This way when θ_0 is 0 degrees, the cracks are aligned and when θ_0 is 90 degrees, the cracks are randomly oriented.

WAVES IN DAMAGED MEDIA

Using the calculated effective moduli, we can predict the elastic wave speeds in cracked media. In order to find the wave speed of plane harmonic waves in direction $\mathbf{L}$, we need to solve the following eigenvalue equation, [14]

$$\det\{A_{ij}-\delta_{ij}\rho v^2\}=0\,. \qquad (5)$$

where, $\mathbf{A} = \mathbf{L}^T\mathbf{C}\mathbf{L}$ is the acoustic tensor, $\mathbf{C}$ is the elastic tensor and $\mathbf{L}$ is a 3×2 direction cosine matrix.

$$[\mathbf{L}] = \begin{bmatrix} l_1 & 0 \\ 0 & l_2 \\ l_2 & l_1 \end{bmatrix} \tag{6}$$

The slowness is the inverse of wave speed:

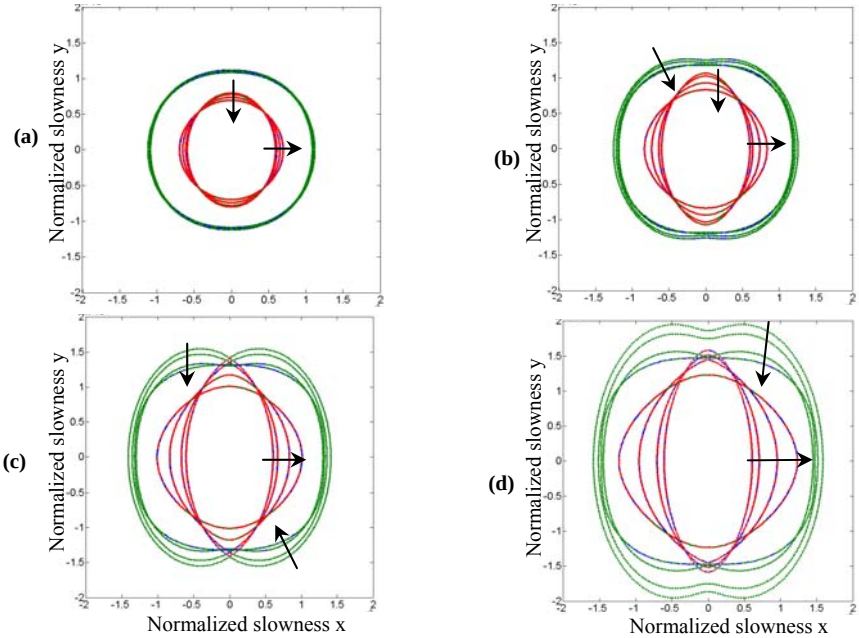

Figure 3. Normalized slowness of waves in cracked media under tension.
The arrows point to the direction where θ_0 increases. (a) η=0.1, (b) η=0.2, (c) η=0.3, (d) η=0.4

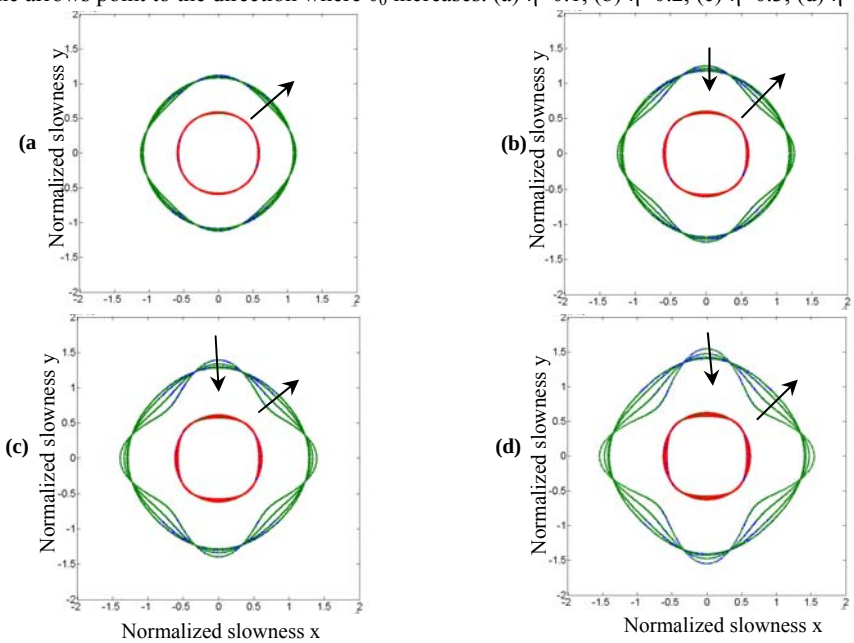

Figure 4. Normalized slowness of waves in cracked media under compression.
The arrows point to the direction where θ_0 increases. (a) η=0.1, (b) η=0.2, (c) η=0.3, (d) η=0.4

$$\mathbf{S}^{(i)}(\mathbf{l}) = \frac{\mathbf{l}}{\boldsymbol{v}^{(i)}} \qquad (7)$$

Fig. 3 shows the normalized inverse of the wave speed (slowness) in the cracked media under tensile loads. Fig. 4 shows slowness under compressive loads. The outside lines are for maximum slowness and the inner lines are for minimum slowness. The arrows show the direction in which θ_0 increases from 0 to 90 degrees.

CONCLUSION AND DISCUSSION

Microcrack damage has a significant effect on the elastic moduli and thus will change the wave propagation within the media. From both figures, it is evident that when η increases, the wave slowness increases (speed decreases). This is due to the fact that as η increases there are more cracks per unit area and the medium becomes less stiff. In addition, when the angular distribution parameter θ_0 decreases, the cracks are more aligned. Therefore, the medium becomes more anisotropic and the slowness diagrams become less circular.

However, we can see that when $\theta_0=90^o$, the figures are not true circles which means the results are not perfectly isotropic. The reason for this is that in the analysis, we have completely decoupled the tension and compression. In reality, the tension and compression moduli have an effect on each other through shear case and should be calculated simultaneously. Currently, we are working on improving the analysis to address this issue.

Comparing Fig. 3 and 4, we can see that as the damage increases, the wave speeds are very different under tensile and compressive loads. As expected. When the medium is loaded in tension, more energy is associated with crack opening (Mode I). Therefore, the modulus decreases more than for the same medium loaded in compression. As a result, under tension the slowness increases more than in compression. If friction were included in this analysis, it would affect the compressive results more than the tension results since compression causes more crack faces contact.

ACKNOWLEDGEMENTS

This research was supported by the United States Army Research Laboratory through the Composite Materials Technology Grant awarded to the Center for Composite Materials

REFERENCES

1. Budiansky B., O'Connell, R.J., Elastic moduli of a cracked solid, Int. J. Sols Strucs, 12, p. 81-97, 1976.
2. Horii, H., Nemat-Nasser, S., Overall Moduli of solid with microcracks: Load-Induced anisotropy, J. Mech. Phys. Solids, 31, # 2, p. 155-171, 1983.
3. Mori T., Tanaka K., Average stress in matrix and average elastic energy of materials with misfitting inclusions. Acta Metall 21, p. 571-574, 1973.
4. Benveniste Y, On the Mori-Tanaka's method in cracked bodies, Mech Res Commun 13, p. 193-201, 1986.
5. Hashin, Z., The differential scheme and its application to cracked materials, J. Mech. Phys. Solids, Vol. 36, #6, p. 719-734, 1988.
6. Aboudi J., Benveniste, Y., The Effective moduli of cracked bodies in plane deformations. Engineering Fracture Mechanics, 26, #2. p. 171-184, 1987.
7. Huang, Y., Hu, K.X., Chandra, A., A generalized self-consistent mechanics method for microcracked solids, J. Mech. Phys. Solids, 42, #8, p. 1273-1291, 1984.
8. Santare, M.H., Crocombe, A.D., Anlas, G., Anisotropic effective moduli of materials with microcracks, Eng. Fracture Mech., 52, #5, p. 833-842, 1995.
9. Zheng, Q.S., Du, D.X., An explicit and universally applicable estimate for the effective properties of multiphase composites which accounts for inclusion distribution , J. Mech. Physics Solids, 49, p. 2765 – 2788, 2001.
10. Sayers C.M., Van Munster, J.G., Microcrack-induced Seismic Anisotropy of Sedimentary Rocks, J. Geophysical Res., 96, #B10, p. 529-533, 1991
11. Sayers, C.M., Kachanov, M., Microcrack-induced elastic wave anisotropy of brittle rocks, J. Geophysical Res., 100, #B3, p. 4149-4156, 1995.
12. Schubnel, A., Gue´guen, Y., Dispersion and anisotropy of elastic waves in cracked rocks, J. Geophysical Res., 108, #B2, p. 2101, 2003.
13. Gueguen, Y., Schubnel, A., Elastic wave velocities and permeability of cracked rocks, Tectonophysics, 370, p. 163-176, 2003.
14. Auld B.A., 1990, Acoustic Fields and Waves in Solids, Volume I, 2nd Edition, Krieger Publ. Co., Malabar, Florida, 435 pp.

CP845, *Shock Compression of Condensed Matter - 2005,*
edited by M. D. Furnish, M. Elert, T. P. Russell, and C. T. White

NUMERICAL CONVERGENCE OF THE COHESIVE ELEMENT APPROACH IN DYNAMIC FRAGMENTATION SIMULATIONS

R. Raghupathy[1], G.A. Gazonas[2], J.F. Molinari[1*], F. Zhou[1]

[1] *Department of Mechanical Engineering, Johns Hopkins University, Baltimore, MD 21218*
[2] *US Army Research Laboratory, Weapons and Materials Research Directorate, Aberdeen Proving Ground, MD 21005*

Abstract. The cohesive element approach is getting increasingly popular for simulations in which a large amount of cracking occurs. Naturally, a robust representation of fragmentation mechanics is contingent to an accurate description of dissipative mechanisms in form of cracking and branching. This paper addresses the issue of energy convergence of the finite-element solution for high-loading rate fragmentation problems. These results provide new insight for choosing mesh sizes and size distributions in two and three-dimensional fragmentation.

Keywords: dynamic crack propagation; crack branching; fragmentation; cohesive element; numerical convergence.
PACS: 46.15.-x, 46.50.+a, 62.20.-x

INTRODUCTION

In ceramic materials, it is known that strength, crack initiation and propagation are affected by the presence of flaws at the micrometer scale. Under dynamic loading conditions, cracks initiate at these flaws, and potentially propagate catastrophically to cause large-scale structural failure. Multiple crack initiate at seemingly random locations and material failure occurs through a complex* communication process of stress-wave interactions between cracks. One of the recent numerical approaches for fragmentation that is easy to implement is that of cohesive element method. Crack branching and fragmentation are natural outcomes of the method. In the creation of new surfaces, each opening cohesive element dissipates a given amount of energy. The total energy dissipated is clearly related to the crack path and mesh convergence. It has been generally observed that for a fixed strain rate, finer meshes lead to higher energy dissipation due to more microcracking [1]. The issue of energy convergence during the cracking process is of fundamental importance as it clearly affects the physical robustness of the numerical methodology, and is the main purpose of the paper.

We briefly describe the finite element methodology including the cohesive element approach (illustrated by 2D crack-branching simulation) and analyze convergence issues in a simplified one-dimensional setting and the implications for extension to multidimensional finite element simulations.

COHESIVE ELEMENT METHODOLOGY

Our adopted framework is the explicit dynamics finite element analysis. The equations of equilibrium are integrated along the time axis by the second-order accurate explicit (Newmark) scheme. For stability of the time integration, the time step Δt must be lower than a critical value,

* corresponding author: molinari@jhu.edu

Δt_{stable}, which is related to the dilatational (the fastest) wave speed and the (smallest) mesh size. We use the initially rigid cohesive law [2] and cohesive elements are added on the fly (dynamic insertion). The initial finite-element mesh is free of cohesive elements, and as the dynamic simulation proceeds, cohesive elements are inserted at locations where the stress exceeds a critical value σ_c.

In addition to σ_c (maximum cohesive force) and δ_c (critical opening displacement), a third parameter G_c, which is not independent of the other two corresponds to the area under the σ_c—δ_c curve and is the fracture energy that is needed to fully open a unit area of crack surface. Resolution of appropriate length and time scales associated with the fragmentation process requires proper choice of the material parameters. Expressions for cohesive zone length α have been obtained by [4,5]. The finite element mesh size must be smaller than α in order to resolve the physics of dynamically failing material near a crack tip. It has also been shown [3] that cohesive elements introduce a time scale into the problem associated with the opening of an isolated micro crack which determines whether a particular externally applied strain rate is perceived as a low strain rate or a high strain rate during the dynamic decohesion process. In order to properly resolve the unloading part of the cohesive law in a dynamic fragmentation simulation, the integration time step must be roughly an order of magnitude smaller than this time scale.

Previously, we obtained probing crack branching results in 3D PMMA plates [6]. For the approach in 2D, similar to Falk *et al* [7] we meshed a h=3mm square block of PMMA with an edge crack of 0.25 mm. Finite-element meshes of different sizes (smaller than the cohesive zone length estimate in [5]) were used.

Crack branching results were obtained for all meshes at sufficiently high energy levels for different loading conditions, indicating the method's robustness. However an increase in total cohesive energy dissipated with mesh refinement, was observed. Closer examination of the cracked surfaces showed increased microcracking and crack path variation with mesh refinement (also observed by Ruiz *et al* [1]) leading us to question the possibility of energy convergence, and mesh-independent microcracking. These questions are addressed in the next section for an idealized 1D setting.

DYNAMIC FRAGMENTATION MODEL

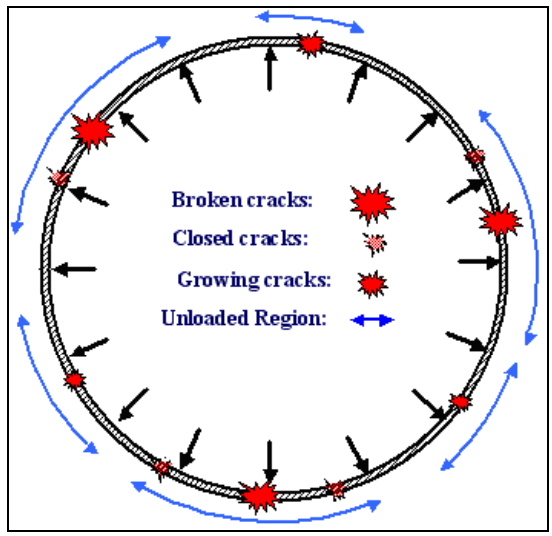

Figure 1: Schematic of dynamic ring fragmenting under explosive loading

For simplicity we consider the most elementary model of an expanding ring (Fig. 1) which has been discussed in earlier work [3,8]. We assume a linearly elastic material and insert 1D initially-rigid cohesive elements upon reaching a critical stress to monitor multiple cracks nucleation, growth, and interactions. The 1D setting allows the use of the method of characteristics to track stress wave interactions in the elastic material and permits high mesh densities at an affordable cost. The results were also compared to finite-element calculations and no significant differences were observed. The ring is loaded explosively with different radial speeds. Fragment statistics are collected when all the fragments are formed. Fragmentation simulations were performed for different mesh sizes (from 128 to 1 million nodes) and for strain rates ranging from 5×10^3 s^{-1} to 5×10^5 s^{-1}.

Figure 2 represents the energy dissipated (curves in solid lines) in the process of cohesive fracture. This includes cohesive elements that have

been either fully or partially damaged. We observe a non-monotonic convergence.

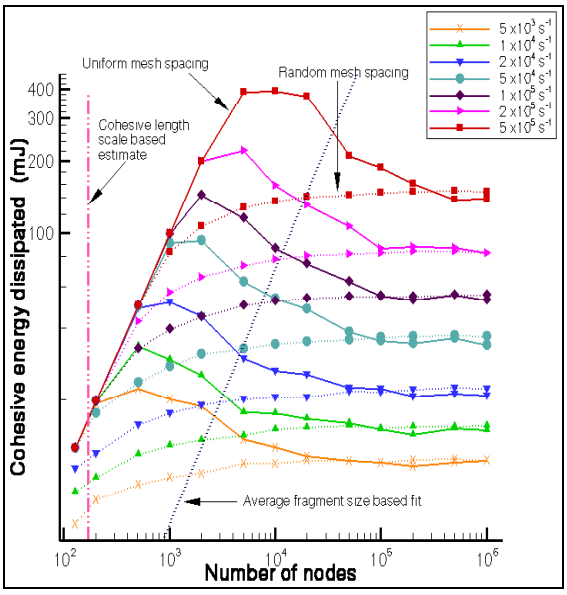

Figure 2: Cohesive energy dependence on mesh size for uniform and random mesh spacing

For coarse meshes the energy dissipated is proportional to the number of nodes in the mesh. This strong mesh dependence clearly indicates that these mesh sizes under resolve the fragmentation process (all the cohesive elements are fully broken and thus the fragment size is mesh size dependent).

The cohesive zone size estimate is shown by the vertical line in Figure 2. Clearly, for this highly dynamic problem, this estimate of mesh size is not satisfying, as it cannot resolve the fragmentation process. In light of this, one may question the validity of using cohesive zone length scale estimates in any dynamic finite-element problem. For illustration, consider the highest strain rate case (5×10^5 s^{-1}). We note that the dissipated energy increases up to 10^4 nodes. Although 10^4 nodes is a relatively small mesh in a 1D setting, its 2D equivalent is 10^8 nodes. Many published results using the cohesive element approach in a multidimensional space have been obtained with smaller meshes. We postulate that observations of energy increase with mesh refinement are due to microcracking being not properly resolved, although the increase may not be linearly proportional to the node number as boundary conditions may deviate from the simple uniaxial state of stress here.

A significant finding of this paper is that for sufficiently large meshes one can properly resolve microcracking. Smooth convergence is observed beyond the peak of the curve This is encouraging as it indicates that although cohesive elements are inserted at many more nodes than necessary most are not severely damaged and do not impact significantly the energy balance of the problem. However it is disturbing to note that this translates to requiring very fine meshes (10^{12} nodes in 2D) beyond any available computational power.

Using a smaller time step did not affect the non-monotonic nature of the curve indicating that perhaps it was not a numerical issue. It was shown previously [8] that a simple universal law (Weibull distribution) captures fragment sizes for all strain rates. Nature wishes to maximize entropy and stays away from uniform fragment sizes due to the inherent randomness associated with generating fragments (which uniform meshes do not capture well). Uniform meshes severely constrain the fragmentation event and its desire to maximize entropy and seems to explain the observed non-monotonic convergence.

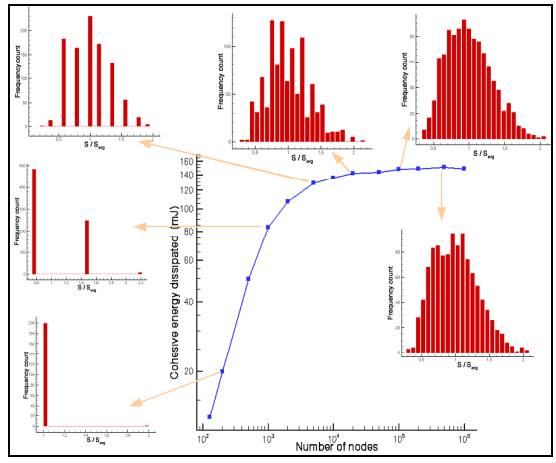

Figure 3: Mesh dependence of fragment size distribution (random mesh spacing) for $5x10^5$ s^{-1}

The curve in dotted lines in Figure 2 represent the results obtained for random meshes obtained by shifting each node by a random amount in between

$\pm$ $0.4h_e$, where h_e is the mesh size in the corresponding uniform mesh. The convergence is now monotonic and, remarkably, it is up to two orders of magnitudes faster. In addition it yields smooth and detailed statistics on fragment sizes (Fig. 3). The required number of nodes and their equivalent in higher dimensions is manageable with parallel simulations. Numerical modeling of fragmentation thus has an odd characteristic: uniform meshes should be avoided at all cost.

Instead of shifting by $\pm 0.4h_e$ we tested for varying degrees of mesh heterogeneity and found that random displacements of nodes by an amount in between $\pm 0.05h_e$ suffice to improve convergence by roughly two orders of magnitude.

As discussed earlier, at least in a 1D setup, cohesive zone estimates such as in [5], lead to meshes too coarse to capture all microcracking events. A key finding of our previous work was that a universal law may be used to capture the dependence of the average fragment size with strain rate. This empirical estimate was proposed as an alternative to Grady's energy-based model [9], which does not take into account wave reflections. Using the average fragment size relation in [10] and Figure 2, we obtain an empirical estimate for required mesh size (shown as dotted line in Figure 2) as:

$$h_e = 0.25(EG_c/\sigma_c^2)\left[1+4.5\left(\frac{\dot{\varepsilon}}{c\sigma_c{}^3/E^2G_c}\right)^{\frac{2}{3}}\right]^{-1}$$

Using this estimate and perhaps others incorporating the time scale, converged 2D fragmentation simulations are within reach. 3D simulations, however, remain too computationally intensive. Rate dependent cohesive laws, for which G_c becomes an increasing function of strain rate, are promising in this regard [11].

CONCLUSIONS

Standard cohesive zone size estimates under resolve the number of nodes necessary for attaining mesh independence in dynamic fragmentation simulations. Substantial computational evidence demonstrates, for the first time, that the cohesive element method converges in an energetic sense. Microcracking events and the ensuing fragment sizes distributions are statistically mesh independent for sufficiently fine meshes. Random mesh spacing led to much faster and smoother convergence than uniform meshes, and that even for very small random perturbations. A simple mesh density estimate based on the dependence of the average fragment size on the strain rate and elastic and fracture material properties is proposed. This estimate provides a clear roadmap for more complex loading conditions including biaxial loading of ceramic plates.

REFERENCES

1. Ruiz, G., Ortiz, M., and Pandolfi, A., Int. J. Numer. Meth. Engng, 52, 97-120, 2001
2. Camacho, G. T., and Ortiz, M., Int. J. Solids Structures, 33, 2899-2938, 1996
3. Zhou, F., Molinari, J. F., Ramesh, K. T., "Effects of Material Properties and Strain Rate on the Fragmentation of Brittle Materials", Int. J. Fracture, (submitted) 2005
4. Rice, J. R., "Fracture, An Advanced Treatise, Vol. II: Mathematical Fundamentals", Liebowitz, H., (Ed.), Academic Press, New York, 191-311, 1968
5. Palmer, A. C., and Rice, J. R., Proc. Roy. Soc. London Ser. A, Vol. 332, 527-548, 1973
6. Zhou, F., and Molinari, J. F., Int. J. Numer. Meth. Engng, 59(1), 2004
7. Falk, M. L., Needleman, A., and Rice, J. R., Journal de Physique IV, Proceedings, pp. Pr.5.43 - Pr.5.50, 2001
8. Zhou, F., Molinari, J. F., Ramesh, K. T., "A finite difference analysis of the brittle fragmentation of an expanding ring", Computational Materials Science, (accepted) 2005
9. Grady, D. E., J. Appl. Phys., 53(1), 1982
10. Zhou, F., Molinari, J. F., Ramesh, K. T., "Characteristic fragment size distribution of dynamically expanding rings", Physical Review Letters, (submitted) 2005
11. Zhou, F., Molinari, J. F., Shioya, T., Engineering Fracture Mechanics, 72, pp. 1383-1410, 2005

NO. OF
COPIES ORGANIZATION

1 (PDF ONLY) DEFENSE TECHNICAL INFORMATION CTR
DTIC OCA
8725 JOHN J KINGMAN RD
STE 0944
FORT BELVOIR VA 22060-6218

1 US ARMY RSRCH DEV & ENGRG CMD
SYSTEMS OF SYSTEMS INTEGRATION
AMSRD SS T
6000 6TH ST STE 100
FORT BELVOIR VA 22060-5608

1 DIRECTOR
US ARMY RESEARCH LAB
IMNE ALC IMS
2800 POWDER MILL RD
ADELPHI MD 20783-1197

3 DIRECTOR
US ARMY RESEARCH LAB
AMSRD ARL CI OK TL
2800 POWDER MILL RD
ADELPHI MD 20783-1197

ABERDEEN PROVING GROUND

1 DIR USARL
AMSRD ARL CI OK TP (BLDG 4600)

NO. OF COPIES ORGANIZATION

1 CECOM
SP & TRRSTRL COMMCTN DIV
AMSEL RD ST MC M
H SOICHER
FT MONMOUTH NJ 07703-5203

1 PRIN DPTY FOR TCHNLGY HQ
US ARMY MATCOM
AMCDCGT
R PRICE
5001 EISENHOWER AVE
ALEXANDRIA VA 22333-0001

1 PRIN DPTY FOR ACQUSTN HQ
US ARMY MATCOM
AMCDCGA
D ADAMS
5001 EISENHOWER AVE
ALEXANDRIA VA 22333-00001

1 DPTY CG FOR RDE HQ
US ARMY MATCOM
AMCRD
5001 EISENHOWER AVE
ALEXANDRIA VA 22333-00001

1 ASST DPTY CG FOR RDE HQ
US ARMY MATCOM
AMCRD
COL S MANESS
5001 EISENHOWER AVE
ALEXANDRIA VA 22333-00001

3 AIR FORCE ARMAMENT LAB
AFATL DLJW
W COOK
D BELK
J FOSTER
EGLIN AFB FL 32542

1 DPTY ASSIST SCY FOR R & T
SARD TT
THE PENTAGON RM 3E479
WASHINGTON DC 20310-0103

3 DARPA
L CHRISTODOULOU
W COBLENZ
S WAX
3701 N FAIRFAX DR
ARLINGTON VA 22203-1714

NO. OF COPIES ORGANIZATION

1 DIRECTOR
US ARMY RESEARCH LAB
AMSRL CS AL TA
2800 POWDER MILL ROAD
ADELPHI MD 20783-1145

3 US ARMY ARDEC
AMSTA AR FSA E
W P DUNN
J PEARSON
E BAKER
PICATINNY ARSENAL NJ
07806-5000

2 US ARMY TARDEC
AMSTRA TR R MS 263
K BISHNOI
D TEMPLETON
WARREN MI 48397-5000

4 COMMANDER
US ARMY BELVOIR RD&E CTR
STRBE N WESTLICH
STRBE NAN
S G BISHOP
J WILLIAMS
FORT BELVOIR VA 22060-5166

3 COMMANDER
US ARMY RESEARCH OFFICE
A RAJENDRAN
J LAVERY
D STEPP
PO BOX 12211
RESEARCH TRIANGLE PARK NC
27709-2211

1 NAVAL RESEARCH LAB
A E WILLIAMS
CODE 6684
4555 OVERLOOK AVE SW
WASHINGTON DC 20375

5 DIRECTOR
LANL
P MAUDLIN
R GRAY
W R THISSELL
A ZUREK
F ADDESSIO
PO BOX 1663
LOS ALAMOS NM 87545

NO. OF COPIES ORGANIZATION

7 DIRECTOR
SANDIA NATL LABS
E S HERTEL JR MS 0819
W REINHART
T VOGLER
R BRANNON MS 0820
L CHHABILDAS MS 1811
M FURNISH MS 0821
M KIPP MS 0820
PO BOX 5800
ALBUQUERQUE NM 87185-0307

3 DIRECTOR
LLNL
M J MURPHY
W TAO L282
A HOLT L290
PO BOX 808
LIVERMORE CA 94550

3 CALTECH
M ORTIZ MS 105 50
G RAVICHANDRAN
T J AHRENS MS 252 21
1201 E CALIFORNIA BLVD
PASADENA CA 91125

2 ARMY HIGH PERFORMANCE
COMPUTING RSRCH CTR
T HOLMQUIST
G JOHNSON
1200 WASHINGTON AVE S
MINNEAPOLIS MN 55415

3 SOUTHWEST RSRCH INST
C ANDERSON
J WALKER
K DANNEMANN
P O DRAWER 28510
SAN ANTONIO TX 78284

1 LIVERMORE SOFTWARE
TECH CORP
J O HALLQUIST
2876 WAVERLY WAY
LIVERMORE CA 94550

1 TEXAS A&M UNIV
DEPT OF MATH
J WALTON
COLLEGE STATION TX 77843

NO. OF COPIES ORGANIZATION

5 UNIV OF NEBRASKA
DEPT OF MECH ENGRG
D ALLEN
F BOBARU
Y DZENIS
G GOGOS
J TURNER
LINCOLN NE 68588

2 JOHNS HOPKINS UNIV
DEPT OF MECH ENGRG
K T RAMESH
F ZHOU
LATROBE 122
BALTIMORE MD 21218

1 WORCESTER POLYTECHNIC INST
MATH SCI
K LURIE
WORCESTER MA 01609

4 UNIV OF UTAH
DEPT OF MATH
A CHERKAEV
E CHERKAEV
T FOLIAS
G MILTON
SALT LAKE CITY UT 84112

1 PENN STATE UNIV
DEPT OF ENGNG SCI & MECHS
F COSTANZO
UNIVERSITY PARK PA 168023

3 UNIV OF DELAWARE
DEPT OF MECH ENGRG
T BUCHANAN
T W CHOU
M SANTARE
126 SPENCER LAB
NEWARK DE 19716

1 UNIV OF DELAWARE
CTR FOR COMPOSITE MTRLS
J GILLESPIE
NEWARK DE 19716

3 SRI INTERNATIONAL
D CURRAN
D SHOCKEY
R KLOPP
333 RAVENSWOOD AVE
MENLO PARK CA 94025

NO. OF COPIES ORGANIZATION

1 VIRGINIA POLYTECHNIC INST
COLLEGE OF ENGRG
R BATRA
BLACKSBURG VA 24061-0219

1 COMPUTATIONAL MECHANICS
CONSULTANTS
J A ZUKAS
P O BOX 11314
BALTIMORE MD 21239-0314

1 KAMAN SCIENCES CORP
D L JONES
2560 HUNTINGTON AVE STE 200
ALEXANDRIA VA 22303

1 APPLIED RSRCH ASSOC
D E GRADY
4300 SAN MATEO BLVD NE
STE A220
ALBUQUERQUE NM 87110

1 INTL RSRCH ASSOC INC
D L ORPHAL
4450 BLACK AVE
PLEASANTON CA 94566

1 AKT MISSION RSRCH CORP
M EL RAHEB
23052 ALCALDE DR
LAGUNA HILLS CA 92653

1 WASHINGTON ST UNIV
SCHOOL OF MECH & MATL ENGRG
J L DING
PULLMAN WA 99164-2920

2 WASHINGTON ST UNIV
INST OF SHOCK PHYSICS
Y M GUPTA
J ASAY
PULLMAN WA 99164-2814

1 ARIZONA STATE UNIV
MECH & ARSPC ENGRG
D KRAJCINOVIC
TEMPE AZ 85287-6106

NO. OF COPIES ORGANIZATION

1 UNIV OF DAYTON RSRCH INST
N S BRAR
300 COLLEGE PARK
MS SPC 1911
DAYTON OH 45469

1 DIRECTOR
USARL
K WILSON
FRENCH DEA 1396
ADELPHI MD 20783-1197

1 TEXAS A&M UNIV
DEPT OF GEOPHYSICS
T GANGI
COLLEGE STATION TX 77843

1 UNIV OF SAN DIEGO
DEPT OF MATH & CMPTR SCI
A VELO
5998 ALCALA PARK
SAN DIEGO CA 92110

1 NATL INST OF STAND & TECH
BLDG AND FIRE RSRCH LAB
J MAIN
100 BUREAU DR MS 8611
GAITHERSBURG MD 20899-8611

1 BUCKNELL UNIV
DEPT OF MECH ENGRG
C RANDOW
LEWISBURG PA 17837

ABERDEEN PROVING GROUND

73 DIR USARL
AMSRD ARL WM
J ALTHOUSE
S KARNA
J MCCAULEY
J SMITH
T WRIGHT
AMSRD ARL WM B
J NEWILL
M ZOLTOSKI
AMSRD ARL WM BA
AMSRD ARL WM BC
P PLOSTINS

NO. OF COPIES ORGANIZATION

AMSRD ARL WM BD
P CONROY
B FORCH
R LIEB
R PESCE RODRIGUEZ
B RICE
AMSRD ARL WM BF
D WILKERSON
AMSRD ARL WM EG
E SCHMIDT
AMSRD ARL WM M
S MCKNIGHT
AMSRD ARL WM MA
R JENSEN
M VANLANDINGHAM
E WETZEL
AMSRD ARL WM MB
M BERMAN
L BURTON
T BOGETTI
W CHOWDHURY
W DE ROSSET
W DRYSDALE
A FRYDMAN
D HOPKINS
L KECSKES
T H LI
M MINNICINO
B POWERS
J TZENG
AMSRD ARL WM MC
R BOSSOLI
S CORNELISON
M MAHER
W SPURGEON
AMSRD ARL WM MD
B CHEESEMAN
E CHIN
B DOOLEY
C FOUNTZOULAS
G GAZONAS
J LASALVIA
P PATEL
J SANDS
C F YEN
AMSRD ARL WM RP
J BORNSTEIN
AMSRD ARL WM SG
T ROSENBERGER
AMSRD ARL WM T
AMSRD ARL WM TA
S SCHOENFELD

NO. OF COPIES ORGANIZATION

AMSRD ARL WM TB
P BAKER
R SKAGGS
J STARKENBERG
AMSRD ARL WM TC
R COATES
K KIMSEY
D SCHEFFLER
S SCHRAML
AMSRD ARL WM TD
S BILYK
T BJERKE
D CASEM
J CLAYTON
D DANDEKAR
M GREENFIELD
K IYER
B LOVE
M RAFTENBERG
E RAPACKI
M SCHEIDLER
S SEGLETES
T WEERASOORIYA
AMSRD ARL WM TE
J POWELL
B RINGERS
G THOMSON

NO. OF COPIES ORGANIZATION

1 DERA
N J LYNCH
WEAPONS SYSTEMS
BUILDING A20
DRA FORT HALSTEAD
SEVENOAKS
KENT TN 147BP
UNITED KINGDOM

1 ERNST MACH INTITUT
H NAHAME
ECKERSTRASSE 4
D 7800 FREIBURG 1 BR 791 4
GERMANY

1 FOA2
P LUNDBERG
S 14725 TUMBA
SWEDEN

1 PCS GROUP
CAVENDISH LABORATORY
W G PROUD
MADINGLEY RD
CAMBRIDGE
UNITED KINGDOM

1 CENTRE D ETUDES DE GRAMAT
J Y TRANCHET
46500 GRAMAT
FRANCE

1 MINISTERE DE LA DEFENSE
DR G BRAULT
DGA DSP STTC
4 RUE DE LA PORTE DISSY
75015 PARIS
FRANCE

1 SPART DIRECTION BP 19
DR E WARINGHAM
10 PLACE GEORGES
CLEMENCEOUX
92211 SAINT CLOUD CEDEX
FRANCE

1 LMT CACHAN
J F MOLINARI
61 AVE DU PRESIDENT WILSON
94235 CACHAN CEDEX
FRANCE

NO. OF COPIES ORGANIZATION

1 TECHNICAL UNIV OF CRETE
G EXADAKTYLOS
DEPT OF MINERAL RES ENGNG
CHANIA CRETE
GREECE

1 ROYAL MILITARY COLLEGE OF SCIENCE
CRANEFIELD UNIV
J MILLETT
SHRIVENHAM SWINDON
SN6 8LA
UNITED KINGDOM

1 UNIV OF MANCHESTER
N K BOURNE
PO BOX 88
SACKVILLE STREET MANCHESTER
M60 1QD UK

1 BEN GURIAN UNIV OF NEGEV
E ZARETSKY
DEPT OF MECH ENG BEER-SHEVA
ISRAEL 84105

2 RUSSIAN ACADEMY OF SCIENCES
INSTITUTE FOR HIGH ENERGY DENSITIES
G I KANEL
S V RAZORENOV
IVTAN IZHORSKAYA 13/19
MOSCOW 127412 RUSSIA

1 INST FUR MATERIALFORSCHUNG II
C TSAKMAKIS
POSTFACH 3640
FORSCHUNGSZENTRUM KARLSRUHE
D 76021 KARLSRUHE
GERMANY

1 TECHNICAL UNIV OF DENMARK
DEPT OF MATHEMATICS
M BENDSOE
2800 LYNGBY
DENMARK

1 TECHNICAL UNIV OF DENMARK
DEPT OF MECH ENGRG
O SIGMUND
2800 LYNGBY
DENMARK

NO. OF
COPIES ORGANIZATION

1 NATL TECH UNIV OF ATHENS
DEPT OF ENG SCI
I VARDOULAKIS
ATHENS 15773
GREECE

1 UNIV OF PATRAS
DEPT OF CIVIL ENGRG
D BESKOS
PATRAS 26500
GREECE

1 ARISTOTLE UNIV
OF THESSALONIKI
DEPT OF MECH & MATLS
E AIFANTIS
THESSALONIKI 54006
GREECE

1 DEMOCRITUS UNIV OF THRACE
DEPT OF CIVIL ENGRG
E GDOUTOS
XANTHI
GREECE

INTENTIONALLY LEFT BLANK.